Chemical Science

ROYAL SOCIETY OF CHEMISTRY

EDGE ARTICLE

View Article Online
View Journal | View Issue

Cite this: *Chem. Sci.*, 2021, **12**, 14254

All publication charges for this article have been paid for by the Royal Society of Chemistry

Coordination-bond-directed synthesis of hydrogen-bonded organic frameworks from metal–organic frameworks as templates†

Jian Su, Shuai Yuan, Yi-Xun Cheng, Zhi-Mei Yang and Jing-Lin Zuo *

Received 21st July 2021
Accepted 10th October 2021

DOI: 10.1039/d1sc03962h

rsc.li/chemical-science

Controlled synthesis of hydrogen-bonded organic frameworks (HOFs) remains challenging, because the self-assembly of ligands is not only directed by weak hydrogen bonds, but also affected by other competing van der Waals forces. Herein, we demonstrate the coordination-bond-directed synthesis of HOFs using a preformed metal–organic framework (MOF) as the template. A MOF (Cu^{I}-TTFTB) based on two-coordinated Cu^{I} centers and tetrathiafulvalene-tetrabenzoate (TTFTB) ligands was initially synthesized. Cu^{I}-TTFTB was subsequently oxidized to the intermediate (Cu^{II}-TTFTB) and hydrated to the HOF product (TTFTB-HOF). Single-crystal-to-single-crystal (SC-SC) transformation was realized throughout the MOF-to-HOF transformation so that the evolution of structures was directly observed by single-crystal X-ray diffraction. The oxidation and hydration of the Cu^{I} center are critical to breaking the Cu–carboxylate bonds, while the synergic corbelled S···S and π···π interactions in the framework ensured stability of materials during post-synthetic modification. This work not only provided a strategy to guide the design and discovery of new HOFs, but also linked the research of MOFs and HOFs.

Introduction

Hydrogen-bonded organic frameworks (HOFs) are a rising class of porous materials that are self-assembled through hydrogen-bonding interactions between organic or metal–organic linkers. With the reversible and flexible nature of hydrogen-bonding connections, HOFs show high crystallinity, easy solution processability, and facile recyclability. These merits stimulate the studies of HOFs as a multi-functional platform in the area of gas storage and separation, molecular recognition, electric/optical materials, chemical sensing, catalysis, and biomedicine.[1–8] Although different methods have been explored to synthesize HOFs including slow solvent evaporation,[9,10] diffusion,[11–13] and solvothermal methods,[14] the controllable synthesis of HOFs remains a challenge. Due to the inherently weak hydrogen bond interactions, the formation of HOFs by self-assembly is subject to the influence of other competing van der Waals force (such as π···π and σ···π interactions) between ligands and solvent molecules. A slight modification of ligands, change of solvents, or reaction temperature may significantly alter the self-assembled products.[15–17] As a result, many attempted syntheses of HOFs in a one-pot reaction may end up with non-porous products formed by closely packed ligands. For comparison, metal–organic frameworks (MOFs) and covalent organic frameworks (COFs), with coordination bonds and covalent bonds, can be rationally designed and synthesized based on reticular chemistry.[18,19] Therefore, it requires a new synthetic method to control the formation of HOFs and enrich their structural diversity.

Templated synthesis has been a vital strategy to construct porous materials such as MOFs and COFs. For example, templated syntheses of MOFs by post-synthetic metalation/demetallation,[20,21] metal exchange,[22–24] or ligand exchange[25–28] have been widely used to obtain targeted functional MOFs with the same structure/topology as the MOF-template. These templated syntheses take advantage of the reversible coordination bonds which can break and reform during post-synthetic modifications. The reversible coordination bonds have also been used to template the synthesis of COFs[29] and porous polymers.[30–32] A representative example has been demonstrated by Yaghi and co-workers, which used the reversible formation/break of Cu^{I}-phenanthroline coordination moieties to construct COFs with woven structures.[29] The copper centers are topologically independent of the weaving within the COF structure and serve as templates for bringing the threads into a woven pattern rather than the more commonly observed parallel arrangement. The weak coordinated Cu^{I} can be removed without breaking the COF structure. These works inspire us to guide the assembly of HOFs using coordination bonds.

To realize the design of coordination-bond-directed HOF synthesis, a MOF based on weak coordination bonds will be

State Key Laboratory of Coordination Chemistry, School of Chemistry and Chemical Engineering, Collaborative Innovation Center of Advanced Microstructures, Nanjing University, Nanjing 210023, P. R. China. E-mail: zuojl@nju.edu.cn

† Electronic supplementary information (ESI) available. CCDC 2082445–2082447. For ESI and crystallographic data in CIF or other electronic format see DOI: 10.1039/d1sc03962h

initially constructed. The weak coordination bonds will be dissociated to form hydrogen bonds while maintaining the spatial arrangement of the organic ligands and the ordered porous structure. Since the MOF-templates can be easily designed by reticular chemistry, the structure and porosity of resulting HOFs can be rationally controlled. In addition to the higher degree of control over the HOF structures, the MOF-templated synthesis may offer promise for the design and discovery of HOFs with unique topologies that are otherwise difficult to form by one-pot synthesis. However, the coordination bonds in most MOFs are usually stronger than the hydrogen bonds in HOFs, which poses a thermodynamic barrier to transform MOFs into HOFs. For example, Zhang and co-workers have reported an isostructural transformation from a hydrogen-bonded network to a MOF on Au(111)/Ag(111) surfaces by replacing the weak N–H···N hydrogen bonds with stronger Ag–N coordination bonds.[33] But the reverse process (*i.e.* replacement of coordination bonds by hydrogen bonds) has never been reported to the best of our knowledge. We propose that the coordination bonds in MOFs could be broken to form hydrogen bonds assisted by the hydration of metal cations.

Herein, a MOF-template (Cu^{I}-TTFTB) has been constructed from the two-coordinated Cu^{I} ions and tetrathiafulvalene-tetrabenzoate (TTFTB) using the solvothermal method. Cu^{I}-TTFTB was stepwise oxidized to the intermediate MOF (Cu^{II}-TTFTB) and hydrated to the HOF product (TTFTB-HOF) by single-crystal-to-single-crystal (SC-SC) transformation. The synergic corbelled S···S and π···π interactions in the framework and the slow hydration reaction ensured the success of SC–SC transformation. The MOF to HOF transformation slightly increased the pore size, and significantly enhanced the electron conductivity by about 3 fold to 2.9×10^{-5} S m^{-1}.

Results and discussion

Crystal structure of the 2-coordinated Cu^{I}-MOF

Cu^{I}-TTFTB was synthesized by the reaction between $Cu(NO_3)_2$ and H_4TTFTB in which Cu^{II} was *in situ* reduced to Cu^{I} by *N*,*N*-dimethylformamide (DMF) solvent under solvothermal conditions. The reduction of Cu^{II} to Cu^{I} during MOF synthesis is well documented in the literature.[34–36] Analysis of the X-ray diffraction data for Cu^{I}-TTFTB revealed that it crystallized in the monoclinic space group C_2/c (Table S1†). The asymmetric unit (Fig. S1†) contains a half Cu^{I} ion, a half H_2TTFTB^{2-}, a half $(CH_3)_2NH_2^{+}$ counterion, and a half free *N*,*N*-dimethylformamide (DMF). The H_2TTFTB^{2-} ligand is coordinated to two Cu^{I} ions through the two carboxylate groups in which all are ligated in a monodentate mode (Fig. 1a). The Cu^{I} ion is two-coordinated with two carboxylate groups from each H_2TTFTB^{2-} (Fig. 1c). The Cu^{I} ion and two neighboring O atoms are in a linear coordination geometry with the Cu–O bond length of 1.835(2) Å, which is comparable to the reported Cu^{I}–carboxylate coordination compounds.[37–40] Hydrogen bonds exist between a pair of OH from uncoordinated carboxylic acids and O from Cu-coordinated carboxylates ($d_{O2–O3A}$ = 2.569 Å (symmetry code A, 3/2 − *x*, 1/2 + *y*, 3/2 − z), ∠O3H3O2 = 173°, Fig. 1b). Overall, the H_2TTFTB^{2-} ligands are assembled by hydrogen bonds into

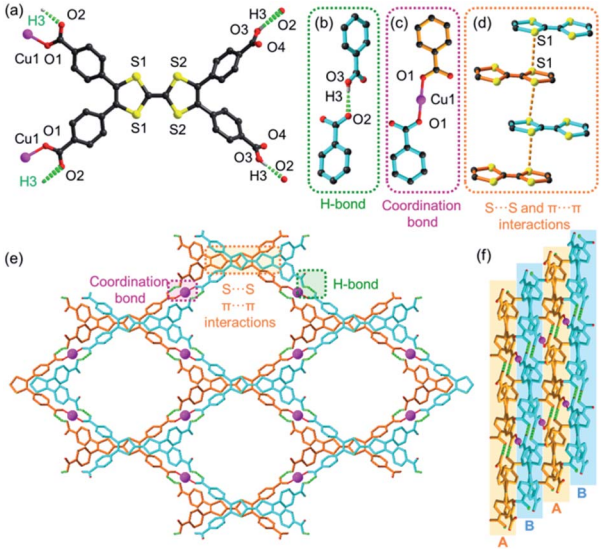

Fig. 1 Crystal structure of Cu^{I}-TTFTB. (a) The structure and coordination environment of H_2TTFTB^{2-}. (b) The hydrogen bond between two carboxylates of H_2TTFTB^{2-}. (c) The coordination bond between Cu^{I} and H_2TTFTB^{2-}. (d) The S···S and π···π interactions between neighboring TTF moieties. (e) The structure of Cu^{I}-TTFTB viewed along the *c*-direction. Two sets of hydrogen-bonded networks are colored blue and yellow. The hydrogen bond within the network, coordination bond between two sets of networks, and S···S/π···π interactions are highlighted by green, violet, and orange. The molecules in the channels are omitted for clarity. (f) The structure of Cu^{I}-TTFTB viewed along the *b*-direction showing the AB stacking mode. Color scheme: Cu, violet; O, red; C, black; S, yellow.

a 2D network with **sql** topology (Fig. 1e), which are further stacked in an AB mode and linked through Cu–O coordination bonds between adjacent planes A and B (Fig. 1f). Meanwhile, the stacked 2D networks are stabilized by S···S and π···π interactions with a S···S distance of 3.792 Å (Fig. 1d). Microporous 1D channels were observed along the crystallographic **c** direction with a diameter of ~12.2 Å (Fig. 1e, and Fig. S2 and S3†). The SQUEEZE calculations in PLATON[41] give a total solvent-accessible volume of 2370.7 $Å^3$ per unit cell, equivalent to 40.5% of the total crystal volume. The porosity of Cu^{I}-TTFTB is slightly higher than that of the transition-metal TTF-based MOF, M_2(TTFTB) (37.9%).[42] Cu^{I}-TTFTB could maintain its morphology in air for at least 19 days (Fig. S4†), but it dissolves in DMF possibly due to the weak hydrogen bonds.

Crystal structure of the HOF obtained by SC-SC transformation

The structural analysis for Cu^{I}-TTFTB reveals that it can be transformed into a HOF if Cu^{I} is removed from the lattice. The transformation of Cu^{I}-TTFTB into the HOF was carried out by incubating crystals of Cu^{I}-TTFTB in water/acetone solution (1 vol%) for 14 days. The color of Cu^{I}-TTFTB crystals changed from red to dark red after the incubation (Fig. S5 and S6†) while the morphology of crystals remains visually intact. By single crystal X-ray diffraction, the resulting crystals are found to be a HOF, namely TTFTB-HOF (Fig. 2). TTFTB-HOF still crystallizes

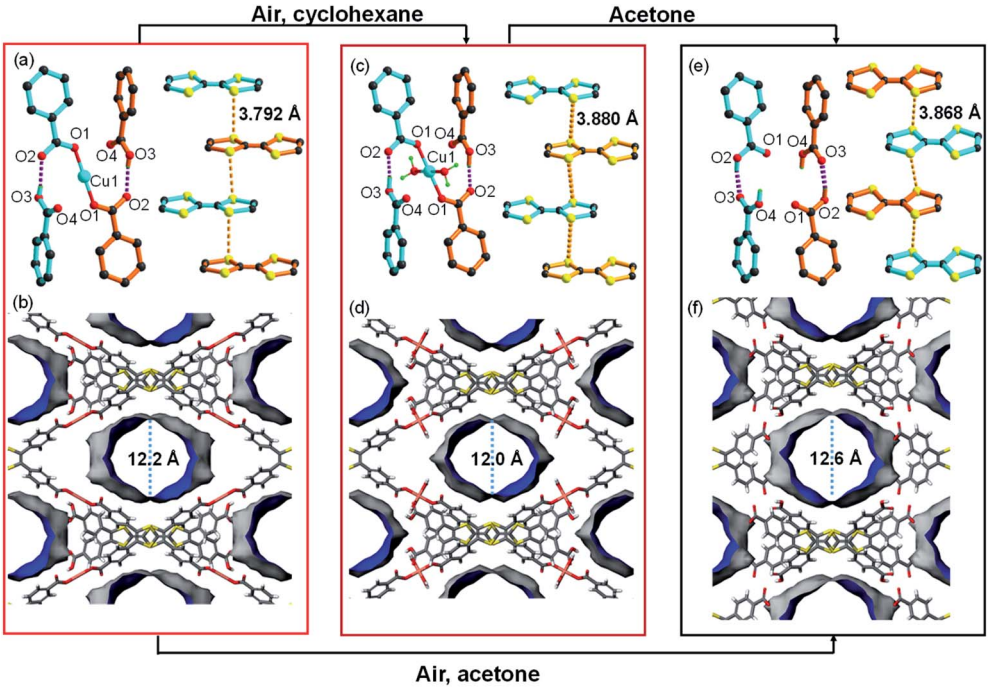

Fig. 2 Single crystal transformation of Cu^{I}-TTFTB to Cu^{II}-TTFTB to TTFTB-HOF. The structure of the Cu center with four adjacent carboxylates and the packing of TTF moieties in Cu^{I}-TTFTB (a), Cu^{II}-TTFTB (c), and TTFTB-HOF (e). The accessible solvent surface of Cu^{I}-TTFTB (b), Cu^{II}-TTFTB (d), and TTFTB-HOF (f) showing the change of cavity sizes upon structural transformation. The molecules in the channels are omitted for clarity. The pore size and accessible solvent surface were calculated based on the N_2 molecule as the probe (kinetic diameter of 3.64 Å).

in the monoclinic space group C_2/c ($a = 20.495$, $b = 34.798$, $c = 8.801$ Å, Table S1†) with comparable cell parameters to those of Cu^{I}-TTFTB ($a = 19.165$, $b = 34.704$, $c = 8.882$ Å). But the Cu^{I} has been removed from the skeleton. The $(CH_3)_2NH_2^+$ counterion was also absent in the crystal structure of TTFTB-HOF (Fig. S7 and S8†), and the charge was presumably balanced by the protonation of two carboxylates. Detailed structural analysis of TTFTB-HOF shows slightly rotated phenyl-carboxylate moieties and slipped TTF moieties. As a result, the hydrogen bond donor⋯acceptor lengths (O2⋯O3) reduced from 2.569 to 2.476 Å accompanied by the increase of S⋯S distance from 3.792 to 3.868 Å, indicating the enhanced hydrogen bond interaction after the removal of Cu^{I}. The pore size of TTFTB-HOF was slightly expanded by ~1 Å compared to that of Cu^{I}-TTFTB, which is in line with the increased *a*-axis length from 19.165 to 20.495 Å. The ideal N_2 adsorption was not obtained owing to the degraded crystallinity of TTFTB-HOF after the activation.

Comparison of reported TTFTB based-HOFs (X-TTF-1,[43] PFC-77, PFC-78, and PFC-79,[44] PFC = porous materials from FJIRSM, CAS) with our TTFTB-HOF in this work shows that there are several differences in the single-crystal structures. Firstly, the reported structures are all crystallized in the space group of $P\bar{1}$, while TTFTB-HOF is in C_2/c. Secondly, the connection types between the carboxylates are different. In the reported structures, a pair of carboxylates forms a typical self-complementary dimer through two hydrogen bonds, while in our TTFTB-HOF structure, each carboxylate pair is connected by one hydrogen bond. At last, the hydrogen bonds showed different bond lengths (defined by the O⋯O distance between the carboxylates). The previously reported HOFs have hydrogen bond-lengths in the range of 2.6–2.8 Å, which are longer than that in TTFTB-HOF (2.48 Å, Table 1). Therefore, the MOF-templated synthesis of TTFTB-HOF may enrich the structural and functional diversity of HOFs.

Both O_2 and H_2O are critical for the structural transformation. Control experiments were conducted in an Ar atmosphere or in dry acetone, which did not yield TTFTB-HOF crystals. To reveal the mechanism of Cu^{I}-TTFTB to TTFTB-HOF transformation, we replaced the water/acetone solution with nonpolar cyclohexane to slow down the hydration. An intermediate was successfully isolated, namely Cu^{II}-TTFTB. Single crystal analysis shows that Cu^{II}-TTFTB crystallizes in the monoclinic space group C_2/c ($a = 18.757$, $b = 35.559$ and $c = 8.899$ Å, Table S1†) with slightly changed cell parameters compared with Cu^{I}-TTFTB ($a = 19.165$, $b = 34.704$ and $c = 8.882$ Å). Interestingly, two water molecules were added to the Cu center which formed a planar 4-coordinated Cu center (Fig. 2c). The Cu^{I} was oxidized into Cu^{II} as reflected by the 4-coordinated

Table 1 Hydrogen bonds in the structure of TTFTB-HOF[a]

Donor-H⋯Acceptor	D-H	H⋯A	D⋯A	Angle (°)
O2–H2⋯O3^{i}	0.82	1.70	2.476(6)	156
C6–H6⋯S1	0.93	2.63	2.998(4)	104
O17–H17⋯O2^{ii}	0.93	2.55	3.248(7)	132

[a] Symmetry transformations used to generate equivalent atoms: *i* (3/2 − *x*, 1/2 + *y*, 3/2 − z), ii (*x*, 1 − *y*, −1/2 + *z*).

square planar geometry and bond lengths (Cu1–O1 = 1.868(7) Å; Cu1–O5(water) = 2.34 (3) Å). The $(CH_3)_2NH_2^+$ counterion was eliminated to balance the charge. The hydrogen bond lengths, defined by the O2···O3 distances (2.569 Å for Cu^I-TTFTB and 2.578 Å for Cu^{II}-TTFTB), did not noticeably change upon Cu oxidation. The packing between TTF moieties slightly slipped leading to the increase of S···S distance from 3.792 Å (Cu^I-TTFTB) to 3.880 Å (Cu^{II}-TTFTB). Compared with Cu^I-TTFTB, the cavity of Cu^{II}-TTFTB shrank along the *a*-direction and expanded along the *b*-direction, indicating the flexibility of the structure.

Characterization of SC–SC transformation

The Pawley refinement against powder X-ray diffraction (PXRD) patterns was carried out for the materials to determine the lattice parameters and confirm the phase purity of bulk materials (Fig. S9, S10 and Table S2†). X-ray photoelectron spectroscopy (XPS) was used to examine the oxidation state change of Cu species in Cu^I-TTFTB, Cu^{II}-TTFTB, and TTFTB-HOF (Fig. S11 and S12†). The Cu species in Cu^I-TTFTB mainly exist in +1 oxidation states with the $Cu2p_{3/2}$ peak located at 931.9 eV.[45] The small peak at 933.8 eV is attributed to the Cu^{II} generated by the surface oxidation of Cu^I-TTFTB. For Cu^{II}-TTFTB, the Cu^{II} peak is increased while the Cu^I peak sharply decreased, suggesting the oxidation of Cu^I to Cu^{II}.

Interestingly, although the crystal structure of TTFTB-HOF indicated the dissociation of Cu from inorganic nodes, the Cu species were not leached out from the crystal. We propose that the dissociated Cu^{II} formed small $Cu(OH)_2 \cdot xH_2O$ particles and they were trapped in the cavity of TTFTB-HOF. Although both Cu^{II}-TTFTB and TTFTB-HOF contain Cu^{II} species, TTFTB-HOF shows an up-shifted $Cu2p_{3/2}$ peak (934.6 eV) compared to that of Cu^{II}-TTFTB (933.8 eV), which can be explained by the different coordination environment of the Cu^{II} center (Fig. S12†).[32] Indeed, the Cu^{II} center is four-coordinated with two water and two carboxylates in Cu^{II}-TTFTB, while Cu^{II} is in a six-coordinated octahedral environment surrounded by OH in $Cu(OH)_2 \cdot xH_2O$. However, there is no characteristic diffraction for $Cu(OH)_2 \cdot xH_2O$ in PXRD patterns, suggesting that $Cu(OH)_2 \cdot xH_2O$ is either amorphous or forms ultra-small nanoparticles (Fig. 3a). The different coordination environments of Cu^{II} in Cu^{II}-TTFTB and TTFTB-HOF may cause shifted $Cu2p_{3/2}$ peak in XPS spectra. Scanning electron microscopy combined with energy-dispersive X-ray spectroscopy (SEM/EDX) further revealed the uniform distribution of Cu and S species throughout the structural transformation (Fig. S13†). After the SC–SC transformation (Cu^I-TTFTB to TTFTB-HOF), the maintained crystal morphology, negligible color change, and the undetected copper element of the supernatant in the inductively coupled plasma (ICP) results, eliminating the possibility of dissolution/recrystallization.

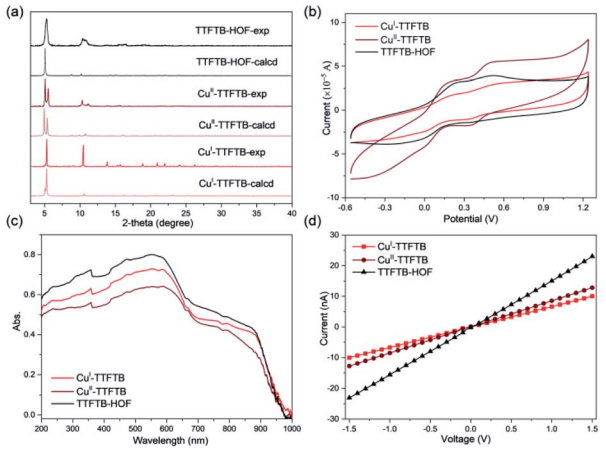

Fig. 3 (a) Experimental and calculated PXRD patterns of Cu^I-TTFTB, Cu^{II}-TTFTB and TTFTB-HOF. The Mercury program allows accounting for preferred orientation of the crystallites, using the March–Dollase parameter. We input a value of 0.65 for this parameter, with orientation to (0 2 0) preferred. (b) Solid state cyclic voltammograms of Cu^I-TTFTB, Cu^{II}-TTFTB, and TTFTB-HOF performed at a scan rate of 400 mV s^{-1}. The experiments were conducted in 0.1 M $LiBF_4$ in CH_3CN electrolyte. Solid-state diffuse reflectance spectra (c) and electrical conducting plots of (d) Cu^I-TTFTB, Cu^{II}-TTFTB and TTFTB-HOF.

Mechanism of SC–SC transformation

Based on the crystal structure and XPS, we proposed a mechanism of the MOF to HOF transformation. The structural transformation was initiated by the oxidation of Cu^I metal nodes into Cu^{II} by O_2. This triggered the coordination of two additional water molecules to the Cu^{II} center. Further hydration of the Cu^{II} center leads to the dissociation of the Cu^{II}–carboxylate coordination bond to form $Cu(OH)_2 \cdot xH_2O$ and protonated carboxylic acids. The oxidation of Cu^I to Cu^{II} is important for the subsequent hydration reaction, as Cu^{II} has a much higher hydration enthalpy (−2161 kJ mol^{-1}) than that of Cu^I (−619 kJ mol^{-1}). This explains the observation that TTFTB-HOF cannot be formed under Ar protection. Water is also required to break the Cu^{II}–carboxylate coordination bond. Cu^{II}-TTFTB readily transformed to TTFTB-HOF in water/acetone solution (1 vol%) within 7 days, whereas this transformation did not happen in dry acetone or cyclohexane for 14 days. The slow hydration ensures the successful SC–SC transformation, while increasing the water concentration to 10 vol% leads to immediate amorphization of MOF-crystals. In addition to O_2 and H_2O, the intrinsic MOF structure is also important for the MOF to HOF transformation in the SC–SC manner. The closely packed TTF moieties stabilized the framework by π···π and S···S interactions, which synergic corbelled the porous structure with hydrogen bonds and maintained the structural intactness after dissociating coordination bonds. In contrast, many MOF-templates in the literature lost the crystallinity after breaking coordination bonds, resulting in amorphous polymer gels or metal oxides/hydroxides.[46–49]

Physical properties

The electrochemical properties of Cu^I-TTFTB, Cu^{II}-TTFTB, and TTFTB-HOF were studied by solid state direct current (DC) cyclic voltammetry (CV) in 0.1 M $LiBF_4$ in CH_3CN (Fig. 3b). The stability of TTFTB-HOF was proved by the remaining PXRD patterns (Fig. S14 and S15†). Upon scanning anodically, two quasi-reversible one-electron processes at ~0.2 and ~0.5 V (*vs.*

Fc/Fc^{+}) were observed. These processes are attributed to the TTF/TTF$^{\bullet+}$ and TTF$^{\bullet+}$/TTF^{2+} redox couples, respectively.[47] The values of the TTF/TTF$^{\bullet+}$ and TTF$^{\bullet+}$/TTF^{2+} redox couples are comparable in the three materials, suggesting that the redox properties of TTF moieties were not affected by the Cu coordination. The location of these two reversible redox processes is consistent with that of the anionic In-TTF-MOFs.[49,50]

The solid-state absorption spectra of Cu^{I}-TTFTB, Cu^{II}-TTFTB, and TTFTB-HOF were obtained to gain insight into the influence of structural transformation on the optical and semiconducting properties. In Cu^{I}-TTFTB, there are two main absorption bands located in the region 200–650 nm (Fig. 3c). This higher energy absorption band is attributed to the $\pi \rightarrow \pi^*$ or $n \rightarrow \pi^*$ transition of the free ligand.[51] In the range of 700–900 nm, the absorption band can be assigned to the partially oxidized TTF$^{\bullet+}$. Using the UV-vis-NIR absorption data, we approximated the bandgap of Cu^{I}-TTFTB, Cu^{II}-TTFTB, and TTFTB-HOF through the Kubelka–Munk function. From the Tauc plots,[52] the band gaps of Cu^{I}-TTFTB, Cu^{II}-TTFTB, and TTFTB-HOF are all approximately 1.29 eV (Fig. S16†). In general, the band gaps of these compounds are comparable to those of radical TTF-MOFs and smaller than those of their neutral counterparts.[53] Correspondingly, the lower optical bandgap of these compounds is attributed to the close S···S interaction in the framework. The bandgap values, which are typical of semiconductors, are such that these materials could potentially be used in photo- and electro-catalysis reactions as well as in microelectronic devices. Furthermore, the electronic conductivity was measured using the *I–V* plots, which revealed that the electronic conductivities of Cu^{I}-TTFTB, Cu^{II}-TTFTB, and TTFTB-HOF are 1.12, 1.17, and 2.90×10^{-5} S m^{-1}, respectively (Table S3†).

Conclusions

In conclusion, we demonstrate the coordination-bond-directed synthesis of HOFs using MOFs as templates. The MOF-to-HOF structural transformation was directly observed by single-crystal X-ray diffraction, which revealed the stepwise oxidation and hydration of the Cu^{I} center leading to the dissociation of Cu–carboxylate bonds. This structural transformation is associated with a change in pore size. The electronic conductivity enhanced by about 3 fold to 2.9×10^{-5} S m^{-1}, as revealed by *I–V* measurements. Considering the diversity of MOF structures, this template strategy is expected to boost the development of HOFs. Further study is in progress in our group to explore the synthesis of functional HOF materials from a variety of MOFs with weak coordination bonds.

Data availability

All experimental supporting data and procedures are available in the ESI.†

Author contributions

J. Z., J. S., and S. Y. conceived and designed the project. J. S., Y.·C., and Z. Y. performed the experiments. S. Y., J. S., and J. Z. drafted the original manuscript. All authors have discussed the results and given approval to the manuscript.

Conflicts of interest

There are no conflicts to declare.

Acknowledgements

This work was supported by the National Basic Research Program of China (2018YFA0306004) and the National Natural Science Foundation of China (No. 21631006 and 21875099). Jian Su thanks the China Postdoctoral Science Foundation (No. 2019M661788).

Notes and references

1 R. B. Lin, Y. He, P. Li, H. Wang, W. Zhou and B. Chen, *Chem. Soc. Rev.*, 2019, **48**, 1362–1389.
2 B. Wang, R. B. Lin, Z. Zhang, S. Xiang and B. Chen, *J. Am. Chem. Soc.*, 2020, **142**, 14399–14416.
3 I. Hisaki, C. Xin, K. Takahashi and T. Nakamura, *Angew. Chem., Int. Ed.*, 2019, **58**, 11160–11170.
4 P. Li, M. R. Ryder and J. F. Stoddart, *Acc. Mater. Res.*, 2020, **1**, 77–87.
5 J. Yang, J. Wang, B. Hou, X. Huang, T. Wang, Y. Bao and H. Hao, *Chem. Eng. J.*, 2020, **399**, 125873.
6 J. Luo, J.-W. Wang, J.-H. Zhang, S. Lai and D.-C. Zhong, *CrystEngComm*, 2018, **20**, 5884–5898.
7 Y. Lin, X. Jiang, S. T. Kim, S. B. Alahakoon, X. Hou, Z. Zhang, C. M. Thompson, R. A. Smaldone and C. Ke, *J. Am. Chem. Soc.*, 2017, **139**, 7172–7175.
8 X. Z. Luo, X. J. Jia, J. H. Deng, J. L. Zhong, H. J. Liu, K. J. Wang and D. C. Zhong, *J. Am. Chem. Soc.*, 2013, **135**, 11684–11687.
9 Q. Huang, W. Li, Z. Mao, L. Qu, Y. Li, H. Zhang, T. Yu, Z. Yang, J. Zhao, Y. Zhang, M. P. Aldred and Z. Chi, *Nat. Commun.*, 2019, **10**, 3074.
10 B. Wang, R. He, L. H. Xie, Z. J. Lin, X. Zhang, J. Wang, H. Huang, Z. Zhang, K. S. Schanze, J. Zhang, S. Xiang and B. Chen, *J. Am. Chem. Soc.*, 2020, **142**, 12478–12485.
11 B. Wang, X. L. Lv, J. Lv, L. Ma, R. B. Lin, H. Cui, J. Zhang, Z. Zhang, S. Xiang and B. Chen, *Chem. Commun.*, 2019, **56**, 66–69.
12 J. M. Taylor, P. J. Dwyer, J. W. Reid, B. S. Gelfand, D.-w. Lim, M. Donoshita, S. L. Veinberg, H. Kitagawa, V. N. Vukotic and G. K. H. Shimizu, *Chem*, 2018, **4**, 868–878.
13 Q. Yin, P. Zhao, R. J. Sa, G. C. Chen, J. Lu, T. F. Liu and R. Cao, *Angew. Chem., Int. Ed.*, 2018, **57**, 7691–7696.
14 Y. Wang, D. Liu, J. Yin, Y. Shang, J. Du, Z. Kang, R. Wang, Y. Chen, D. Sun and J. Jiang, *Chem. Commun.*, 2020, **56**, 703–706.
15 Y. Suzuki, N. Tohnai, A. Saeki and I. Hisaki, *Chem. Commun.*, 2020, **56**, 13369–13372.
16 T. Takeda, M. Ozawa and T. Akutagawa, *Cryst. Growth Des.*, 2019, **19**, 4784–4792.

17 X. Jiang, X. Cui, A. J. E. Duncan, L. Li, R. P. Hughes, R. J. Staples, E. V. Alexandrov, D. M. Proserpio, Y. Wu and C. Ke, *J. Am. Chem. Soc.*, 2019, **141**, 10915–10923.
18 O. M. Yaghi, *ACS Cent. Sci.*, 2019, **5**, 1295–1300.
19 R. Freund, S. Canossa, S. M. Cohen, W. Yan, H. Deng, V. Guillerm, M. Eddaoudi, D. G. Madden, D. Fairen-Jimenez, H. Lyu, L. K. Macreadie, Z. Ji, Y. Zhang, B. Wang, F. Haase, C. Woll, O. Zaremba, J. Andreo, S. Wuttke and C. S. Diercks, *Angew. Chem., Int. Ed.*, 2021, **60**, DOI: 10.1002/anie.202101644.
20 M. C. Das, S. Xiang, Z. Zhang and B. Chen, *Angew. Chem., Int. Ed.*, 2011, **50**, 10510–10520.
21 S. Yuan, Y. P. Chen, J. Qin, W. Lu, X. Wang, Q. Zhang, M. Bosch, T. F. Liu, X. Lian and H. C. Zhou, *Angew. Chem., Int. Ed.*, 2015, **54**, 14696–14700.
22 C. K. Brozek and M. Dinca, *Chem. Soc. Rev.*, 2014, **43**, 5456–5467.
23 L. Liu, L. Li, J. A. DeGayner, P. H. Winegar, Y. Fang and T. D. Harris, *J. Am. Chem. Soc.*, 2018, **140**, 11444–11453.
24 B. Garai, V. Bon, S. Krause, F. Schwotzer, M. Gerlach, I. Senkovska and S. Kaskel, *Chem. Mater.*, 2020, **32**, 889–896.
25 C. Liu, C. Zeng, T. Y. Luo, A. D. Merg, R. Jin and N. L. Rosi, *J. Am. Chem. Soc.*, 2016, **138**, 12045–12048.
26 J. A. Boissonnault, A. G. Wong-Foy and A. J. Matzger, *J. Am. Chem. Soc.*, 2017, **139**, 14841–14844.
27 L. Liu, L. Li, M. E. Ziebel and T. D. Harris, *J. Am. Chem. Soc.*, 2020, **142**, 4705–4713.
28 L. Feng, K. Y. Wang, G. S. Day and H. C. Zhou, *Chem. Soc. Rev.*, 2019, **48**, 4823–4853.
29 Y. Liu, Y. Ma, Y. Zhao, X. Sun, F. Gandara, H. Furukawa, Z. Liu, H. Zhu, C. Zhu, K. Suenaga, P. Oleynikov, A. S. Alshammari, X. Zhang, O. Terasaki and O. M. Yaghi, *Science*, 2016, **351**, 365–369.
30 T. Ishiwata, Y. Furukawa, K. Sugikawa, K. Kokado and K. Sada, *J. Am. Chem. Soc.*, 2013, **135**, 5427–5432.
31 K. Chen and C. D. Wu, *Angew. Chem., Int. Ed.*, 2019, **58**, 8119–8123.
32 X. Wang, M. J. Dong, K. Chen, Z. K. Liu and C. D. Wu, *Chem. Commun.*, 2021, **57**, 1348–1351.
33 D.-D. Zhou, J. Wang, P. Chen, Y. He, J.-X. Wu, S. Gao, Z. Zhong, Y. Du, D. Zhong and J.-P. Zhang, *Chem. Sci.*, 2021, **12**, 1272–1277.
34 O. M. Yaghi and H. Li, *J. Am. Chem. Soc.*, 1995, **117**, 10401–10402.
35 S. M. F. Lo, S. S. Y. Chui, L.-Y. Shek, Z. Lin, X. X. Zhang, G.-h. Wen and I. D. Williams, *J. Am. Chem. Soc.*, 2000, **122**, 6293–6294.
36 C. Hua, P. Turner and D. M. D'Alessandro, *Dalton Trans.*, 2015, **44**, 15297–15303.
37 P. F. Rodesiler and E. L. Amma, *J. Chem. Soc., Chem. Commun.*, 1974, 599.
38 T. Sugiura, H. Yoshikawa and K. Awaga, *Inorg. Chem.*, 2006, **45**, 7584–7586.
39 Y. Sevryugina, O. Hietsoi and M. A. Petrukhina, *Chem. Commun.*, 2007, 3853–3855.
40 O. Hietsoi, C. Dubceac, A. S. Filatov and M. A. Petrukhina, *Chem. Commun.*, 2011, **47**, 6939–6941.
41 A. L. Spek, *Acta Crystallogr., Sect. C: Struct. Chem.*, 2015, **71**, 9–18.
42 S. S. Park, E. R. Hontz, L. Sun, C. H. Hendon, A. Walsh, T. Van Voorhis and M. Dinca, *J. Am. Chem. Soc.*, 2015, **137**, 1774–1777.
43 I. Hisaki, N. Q. E. Affendy and N. Tohnai, *CrystEngComm*, 2017, **19**, 4892–4898.
44 X. Y. Gao, Y. L. Li, T. F. Liu, X. S. Huang and R. Cao, *CrystEngComm*, 2021, **23**, 4743–4747.
45 N. T. Bui, H. Kang, S. J. Teat, G. M. Su, C. W. Pao, Y. S. Liu, E. W. Zaia, J. Guo, J. L. Chen, K. R. Meihaus, C. Dun, T. M. Mattox, J. R. Long, P. Fiske, R. Kostecki and J. J. Urban, *Nat. Commun.*, 2020, **11**, 3947.
46 T. Ishiwata, K. Kokado and K. Sada, *Angew. Chem., Int. Ed.*, 2017, **56**, 2608–2612.
47 Z. Wang, A. Blaszczyk, O. Fuhr, S. Heissler, C. Woll and M. Mayor, *Nat. Commun.*, 2017, **8**, 14442.
48 S. Guo, Y. Zhao, H. Yuan, C. Wang, H. Jiang and G. J. Cheng, *Small*, 2020, **16**, e2000749.
49 J. Su, W. He, X.-M. Li, L. Sun, H.-Y. Wang, Y.-Q. Lan, M. Ding and J.-L. Zuo, *Matter*, 2020, **2**, 711–722.
50 J. Su, S. Yuan, H. Y. Wang, L. Huang, J. Y. Ge, E. Joseph, J. Qin, T. Cagin, J. L. Zuo and H. C. Zhou, *Nat. Commun.*, 2017, **8**, 2008.
51 P. M. Usov, C. Fabian and D. M. D'Alessandro, *Chem. Commun.*, 2012, **48**, 3945–3947.
52 J. Tauc, R. Grigorovici and A. Vancu, *Phys. Status Solidi B*, 1966, **15**, 627–637.
53 J. Su, T. H. Hu, R. Murase, H. Y. Wang, D. M. D'Alessandro, M. Kurmoo and J. L. Zuo, *Inorg. Chem.*, 2019, **58**, 3698–3706.